Available online at www.sciencedirect.com
SCIENCE DIRECT®
Journal of Nuclear Materials 348 (2006) 181–190
journal of nuclear materials
www.elsevier.com/locate/jnucmat

Comprehensive investigation of the corrosion state of the heat exchanger tubes of steam generators. Part I. General corrosion state and morphology

K. Varga [a,*], Z. Németh [a], A. Szabó [a], K. Radó [a], D. Oravetz [b], Z. Homonnay [c], J. Schunk [d], P. Tilky [d], F. Kőrösi [e]

[a] Department of Radiochemistry, University of Veszprém, P.O. Box 158, H-8201 Veszprém, Hungary
[b] Department of Silicate and Materials Engineering, University of Veszprém, P.O. Box 158, H-8201 Veszprém, Hungary
[c] Department of Nuclear Chemistry, Eötvös University, P.O. Box 32, H-1518 Budapest, Hungary
[d] Paks NPP Ltd., P.O. Box 71, H-7031 Paks, Hungary
[e] Department of Physics and Process Control, Szent István University, Páter Str. 1, H-2100 Gödöllő, Hungary

Received 8 October 2003; accepted 16 September 2005

Abstract

The present work, constituting the first part of a series of two, deals with a systematic investigation of the general corrosion state of 22 heat exchanger tubes originating from different steam generators of the Paks NPP (Hungary). While the passivity of the inner surface of the stainless steel tube specimens was studied by voltammetry, the morphology and chemical composition of the oxide layer formed on the surfaces were analyzed by SEM–EDX method. Based on the measured corrosion characteristics (corrosion rate, thickness and chemical composition of the protective oxide layer) a strong dependence of these parameters on the decontamination history of the steam generators was revealed. It is well documented that the chemical decontamination carried out by a non-regenerative version of the AP-CITROX procedure does exert, on the long run, a detrimental effect on the corrosion resistance of steel surfaces. Therefore, process restrictions and modifications to minimize corrosion damages have be defined.

PACS: 82.55.+e; 81.65.Kn

1. Introduction

In accordance with international trends, the life-cycle prolongation of the nuclear reactors of type VVER-440/213 at Paks NPP is a fundamental issue in the energy policy of Hungary. Recent investigations [1] have shown the potential for an additional 20–25 year operation cycle over the 30 years, predicted earlier. This possibility should not be an underestimated resource for the development of the national economy.

Long lasting and continuous availability of the electricity supply for the industry and community

* Corresponding author. Tel./fax: +36 88 427 681.
E-mail address: vargakl@almos.vein.hu (K. Varga).

0022-3115/$ - see front matter © 2005 Elsevier B.V. All rights reserved.
doi:10.1016/j.jnucmat.2005.09.012

as well as demand for high level service of the consumers at an internationally competitive price require enhanced power production and the longest possible life-cycle of the energy production units together with the maximum operation safety. In the enhancement of the power capacity and/or a possible extension of the life-cycle, the contamination and corrosion state of the steam generators (SG) of the VVER 440/213 type pressurized water reactors are considered as being one of the decisive factors (see [1–4] and references therein). The design of these energy production units, however, does not allow the replacement of horizontal SGs to be considered. Therefore, the replacement of even one SG would result in unacceptably high production loss and investment cost. Some years ago, the primary and secondary circuit water chemistry data, and the corrosion effects of the chemical decontamination procedures performed at NPP Paks, made it clear that an overall estimation of the corrosion state of the steam generators, i.e. the preparation of a so-called 'corrosion map' is inevitable. This 'corrosion map' takes a survey of the corrosion features of the heat exchanger tubes made of austenitic stainless steel in the SGs.

Owing to the fact that there are no investigation methods available for the in situ monitoring of the inner and outer surfaces of heat exchanger tubes, a research project based on sampling as well as on ex situ electrochemical and surface analytical measurements was launched in the year 2000. Investigation of the corrosion state of 22 steel samples originating from locations in the steam generators of Paks NPP (24 SGs altogether for the 4 reactors) has been performed [5,6]. (Selection of the sampling locations and the number of samples were restricted by production needs.) Although numerous studies dealing with the corrosion features, structure and composition of oxide layers formed on the surfaces of the heat exchanger tubing of various SGs have been published (see e.g. [3,4,7–14] and references therein), only very limited information on the detrimental corrosion effects of the AP-CITROX chemical decontamination technology is available in the relevant literature [4,7–9,12–14]. The applied version of the AP-CITROX procedure is an eight-step process, including an oxidizing pre-treatment of the surface with alkaline potassium permanganate followed by washing with a concentrated mixture of citric and oxalic acids to remove the contaminated surface layer [7,8]. The industrial use of this rather corrosive technology has raised the question of its effect on the corrosion resistance of the austenitic stainless steel. Moreover, it has become essential to understand the corrosion phenomena as being developed in the long run.

The aim of the present work is therefore to summarize the experimental findings on the surface characteristics (passivity, morphology, chemical composition and structure, phase composition) of the steel specimens provided by the Paks NPP Ltd. This paper, which is the first part of a series of two, presents voltammetric and SEM–EDX results that reveal the general corrosion state, morphology and chemical composition of the inner surfaces (primary circuit side) of heat exchanger tubes.

2. Experimental section

2.1. Preparation of the samples

The experiments have been performed on 22 austenitic stainless steel specimens (type: 08X18H10T (GOST 5632-61) which correspond to AISI 321 and DIN 1.4541, outer diameter: 16 mm, average wall thickness: 1.6 mm) originating from different SGs of Paks NPP. The sampling locations were selected in a way that the corrosion/decontamination history of the samples represents as many different cases as possible while not interfering the operation schedule of the reactors. The main characteristics of the samples are given in Table 1. The surface decontamination procedure (where done) was carried out at Paks NPP in real plant environment, according to the AP-CITROX technology [7,8].

For the voltammetric and SEM–EDX studies, 20 mm long pieces were sliced from the tube samples. The tube pieces were cut into two halves along their axes and even flattened gently for voltammetric measurements. In order to protect the oxide layer on the specimens from possible chemical effect of organic solvents, the surfaces were not degreased. The corrosion properties of the inner surfaces of the stainless steel samples were analyzed using electrochemical, surface spectroscopic and microscopic methods.

2.2. Investigation of the corrosion state of tube specimens by voltammetry

The passivity of the tube samples was studied by potentiostatic polarization method. The experiments were conducted using a computer controlled

Table 1
Main characteristics of the specimens

Sample	Year of decontamination	Year of sampling	Year of investigation
1	2001	2002	2002
2	2001	2002	2003
3	1996, 1997	2001	2001
4	1996	2000	2000
5	1996	1997	2003
6	2001	2002	2002
7	2001	2002	2002
8	2001	2003	2003
9	2001	2002	2002
10	–	1999	2001
11	2001	2002	2002
12	2001	2001	2001
13	1993	2000	2000
14	–	2000	2000
15	–	2003	2003
16	–	1999	2003
17	–	2003	2003
18	–	2001	2001
19	–	1998	2001
20	–	2000	2000
21	–	2001	2001
22	–	1982	2001

(–): Not decontaminated samples.

VoltaLab 40 (RADIOMETER) type electrochemical measuring system. To perform these investigations, a special electrochemical cell was developed [8]. In the course of potentiostatic polarization experiments the potential (E) of the specimen (working electrode) was continuously shifted towards anodic direction at a constant rate of 10 mV min^{-1} and the current density (i) related to the inner surface area of the specimen was recorded. The measurements were carried out in deoxygenated boric acid solution ($c = 12$ g dm^{-3}) in argon gas ambient (99.999 v/v% Ar). The scheme of the measuring system, the detailed experimental procedure and the determination of the corrosion parameters (such as corrosion potential (E_c), corrosion current density (i_c), and corrosion rate (v_c)) derived by the so-called first Stern method have been described in our earlier papers [5,8]. The first Stern method is based on seeking the Tafel lines (anodic and cathodic ones) on the $\log(i) = f(E)$ voltammetric curve. The curve must have a potential value for which the measured current is equal to zero. The intercept of the Tafel lines extrapolated at the zero current potential determines a point where the coordinates of E_c and i_c can be identified. The corrosion rate was calculated from the i_c value by using the well-known relationship detailed in [8]. The average value of the passivity current density (i_{pass}) was also determined in the potential range of 0.40–0.80 V. The electrode potential values quoted in this paper are given on the saturated calomel electrode (SCE) scale.

2.3. Systematic study of the surfaces by SEM–EDX method

The morphology and chemical composition of the oxide layer on the inner surfaces of the 22 stainless steel specimens were studied by scanning electron microscopy (SEM), equipped with an energy dispersive X-ray microanalyzer (EDX) (Type: JEOL JSM-50A, controlled with Röntec EDR 288 software). In case of each specimen having a length of 20 mm, two different surface areas were studied. The comparative evaluation of the surface morphology was done by analyzing the SEM micrographs obtained at two different magnifications, $M = 3000\times$ and $M = 1000\times$. The chemical composition of the sample surfaces was determined on at least two different areas of 1 mm^2 by EDX method. Taking into consideration the average atomic number of the main alloying components of austenitic stainless steel and the energy of the in-coming electrons, the specific radius of the so-called 'excited depth' for the EDX analysis could be estimated and found to be about 1.5 μm.

The metallographic cross-sections of tube specimens were also prepared and studied to evaluate the thickness of the oxide layer. In addition, the SEM images of the metallographic cross-sections were background compensated and shading corrected, with low pass Sobel edge enhancement, Macleod filters being applied [15,16]. Geometric calibration, qualitative mapping and quantified parameters (total oxide layer area, area of the oxide layer of low and high average atomic number, area of crack) were analyzed on the images by the image processing toolbox of Matlab (6.5.0. version) and the Iman 2 (β version) programs [17]. Matlab (6.5.0 version) Statgraphics plus 5 programs [18] were used for modeling the volumes and the weight of the oxide layers grown-on heat exchanger tubes of the steam generators. In view of fit tests performed by empirical distribution function statistics, amorphous, crystalline and total oxide weights formed on heat exchanger tubes of steam generators can be modeled adequately by logistic, lognormal and γ distributions with a $\geqslant 90\%$ confidence, respectively.

3. Results

3.1. Investigation of the corrosion state of tube specimens by voltammetry

The potentiostatic polarization curves measured in boric acid solution at the inner surface of the stainless steel specimens originating from different steam generators of the Paks NPP are shown in Figs. 1–3. The classification of the samples into these figures was done more or less according to their decontamination history. The curves presented were evaluated and the E_c, i_c, v_c and i_{pass} values for all specimens were calculated. The main corrosion parameters are summarized in Table 2.

As clearly seen from the corrosion data compiled in Table 2, the inner surfaces of all samples studied have passive character in a wide potential interval next to the corrosion potential. The calculated corrosion rates are very low, and the corrosion current densities do not exceed the value of $i_c = 4 \times 10^{-7}$ A cm^{-2}. The passivity current densities not higher

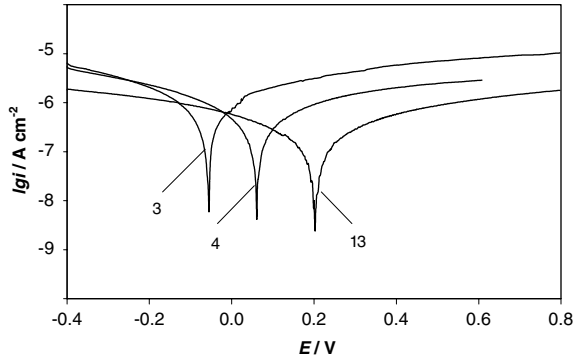

Fig. 1. Potentiostatic polarization curves measured at the inner surface of sample nos. 3, 4 and 13 in boric acid solution ($c = 12$ g dm^{-3}). Scan rate: 10 mV min^{-1}.

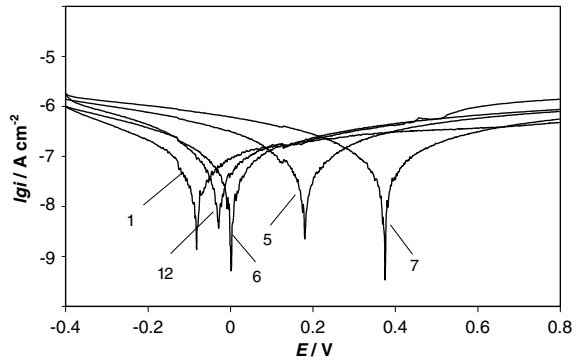

Fig. 2. Potentiostatic polarization curves measured at the inner surface of sample nos. 1, 5, 6, 7, and 12 in boric acid solution ($c = 12$ g dm^{-3}). Scan rate: 10 mV min^{-1}.

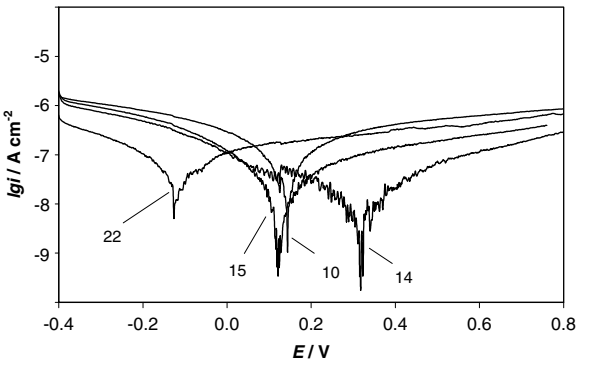

Fig. 3. Potentiostatic polarization curves measured at the inner surface of sample nos. 10, 14, 15 and 22 in boric acid solution ($c = 12$ g dm^{-3}). Scan rate: 10 mV min^{-1}.

Table 2
Corrosion parameters determined from voltammetric curves shown in Figs. 1–3

Sample	Determined corrosion parameters			
	Corrosion potential (E_c), (mV)	Corrosion current (i_c) (nA cm^{-2})	Corrosion rate (v_c) (μm year^{-1})	Passivity current density (i_p) (μA cm^{-2})
1	−82.8	35.0	0.4	0.50
2	−64.0	38.5	0.4	0.35
3	−55.7	300.4	3.5	10.63
4	60.5	335.0	3.9	>1
5	175.5	48.8	0.6	1.1
6	0.7	37.7	0.4	0.83
7	371.3	37.4	0.4	0.38
8	87.5	37.6	0.4	1.00
9	−64.8	37.5	0.4	<1
10	143.7	40.7	0.5	0.81
11	307.6	60.2	0.7	0.92
12	−30.9	49.3	0.6	1.18
13	200.8	160.0	1.8	<1
14	312.2	25.0	0.3	<1
15	114.3	19.3	0.2	0.27
16	249.9	11.6	0.1	0.20
17	404.2	5.1	0.1	0.16
18	−115.7	70.4	0.8	1.81
19	119.4	33.4	0.4	0.55
20	−15.9	–	<1.8	<1
21	−68.4	63.3	0.7	1.86
22	−126.5	35.1	0.4	0.65

than $i_{pass} = 1 \times 10^{-5}$ A cm^{-2} attest the above statement, too. (It should be noted that the voltammetric experiments were conducted *at room temperature in a model solution of the primary coolant*. Consequently, there is no real significance of the measured corrosion potential relative to the actual plant environment in which the oxide film was grown.)

A closer inspection of the data, however, reveals that the potentiostatic polarization behavior of the samples 3, 4 and 13 in Fig. 1 differs significantly from the others. The average corrosion rates (i_c) of their inner surface is well above the values observed for the other samples (see Table 2). A common characteristic for these samples (having the weakest corrosion resistance) as compared to the others is that they were decontaminated a few years before the sampling – in some cases more than one decontamination cycle – by the AP-CITROX technology at Paks NPP.

Sample 12 was also decontaminated, but immediately before the cutting procedure, so the parameters characterizing its passivity are still favorable. (Let us note here that the last step of the AP-CITROX procedure is a passivation treatment using H_2O_2.) Similarly, the data derived from the potentiostatic polarization curves in Fig. 2 confirm that the corrosion parameters of the samples decontaminated in 2001 and sample 5 decontaminated in 1996 – about one or two year before cutting – are as good as the ones never decontaminated earlier. The average corrosion rates of the inner surfaces of samples 1, 2, 6–9 and 11 can be qualified similarly to the samples showing excellent corrosion resistance (e.g. the inactive reference sample (22) and samples 10, 14–21) in Fig. 3. The latter samples were never decontaminated and so their average corrosion rates are extremely low ($v_c \leqslant 0.8$ μm year^{-1}), even better than the data which were measured by the Russian reactor designers for the stainless steel type 08X18H10T (GOST5632-61) in aqueous solutions at temperatures of 280–350 °C [19].

Applying voltammetric data (E_c, i_c, v_c and i_{pass}) compiled in Table 2, an Euclidean sample space was built, where cluster analysis was performed in order to identify and classify similar characteristics of the samples and thereby making inference upon their corrosion states. (Euclidean sample space where the data are interpreted by their Euclidean distance; see [20] and text to Fig. 4(A)). Three clusters were identified. The obtained dendogram and cluster scatterplot are delineated in Fig. 4(A) and (B).

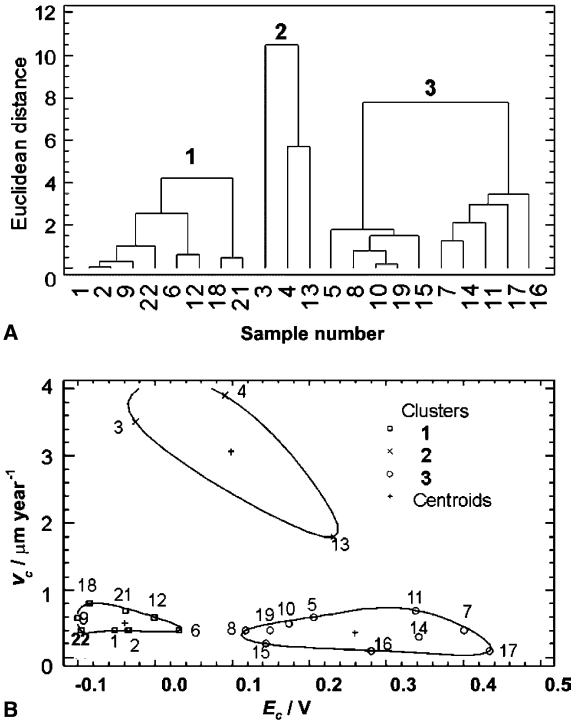

Fig. 4. (A) A cluster analysis dendogram for the samples using voltammetric data. (*The various distances between the vectors in a data matrix are defined as Euclidean distance* [20]). (B) A cluster scatterplot, where the abscissa depicts the corrosion potential and the ordinate plots the corrosion rate.

Sample Nos. 1, 2, 9, 22, 6, 12, 18, 21 (38.10%) belong in the first cluster; 3, 4, 13 (14.29%) in the second; while 5, 8, 10, 19, 15, 7, 14, 11, 17, 16 samples in the third one with highest share of 47.62%. The first cluster, into which the reference sample #22 was classified to, has a cluster centroid of minus 69.0 mV corrosion potential, 45.8 nA cm^{-2} corrosion current density, 1.01 μA cm^{-2} passivity current density and that of 0.51 μm year^{-1} corrosion rate. The samples that pertained to the second cluster were subjected to decontamination by AP-CITROX technology more than two years ago. These samples exhibit the highest i_c, i_{pass} and v_c centroids of 265.1 nA cm^{-2}, 4.24 μA cm^{-2} and 3.01 μm year^{-1}, respectively. Circa 50% of the samples were categorized into the third cluster into which never contaminated (and a few of the one or two years ago contaminated) samples were compartmentalized. This group had the highest E_c of 228.56 mV, and the lowest i_c, i_{pass} and v_c of 31.9 nA cm^{-2}, 0.63 μA cm^{-2} and 0.37 μm year^{-1}, respectively.

4. Systematic study of the surfaces by SEM–EDX method

The measured SEM–EDX data have proved that the samples decontaminated earlier, and found exceptional by voltammetry (Nos. 3, 4 and 13 in Table 1) have very similar surface characteristics. A typical SEM image (actually that of sample 4) representing this group of samples is shown in Fig. 5. As can be seen, the protective oxide layer grown-on the surface of these samples is compact and thick, nevertheless contains many cracks and scattered deep damages. No presence of any deposited crystals can be identified on top of the grown-on oxides. The EDX spectrum in Fig. 5 reveals a surface composition strongly enriched in Ni and especially in Cr as compared to the bulk steel. The SEM micrograph of the cross-section shown in Fig. 5 reveals that the thickness of the grown-on oxide layer is up to 11 μm and the outermost region of the oxide film exhibits amorphous character. (This latter statement is confirmed by conversion electron mössbauer spectroscopy (CEMS) and XRD results to be discussed in Part 2 of this series.)

On the inner surface of the samples, which were decontaminated about one or two years before sampling (Nos. 1, 2, 5–9 and 11) – a medium thick or thick grown-on oxide layer having basically amorphous character ('hybrid' structure) can be detected. There are no any crystalline deposits on the surfaces, and the chromium enrichment in the oxide layers of various specimens is different but significant. Some nickel enrichment can also be measured on the most samples. Some representative findings characterizing the surface properties of this group are demonstrated in Fig. 6 showing results obtained for sample 7.

The SEM and EDX results characterizing the inner surface of sample No. 12 (decontaminated immediately before the cutting procedure) are shown in Fig. 7. The SEM micrograph reveals that the surface layer seen on this sample is compact. The oxide layer grown-on the base alloy looks rather homogeneous, on which large deposited crystals can sparsely be observed. The size of some crystals exceeds 10 μm. The EDX spectrum demonstrates little Ni and Cr enrichment relative to Fe, *and*, *surprisingly*, *the oxide film is contaminated by significant amount of manganese*. The SEM micrograph of the metallographic cross-section confirms that the thickness of the grown-on oxide layer is

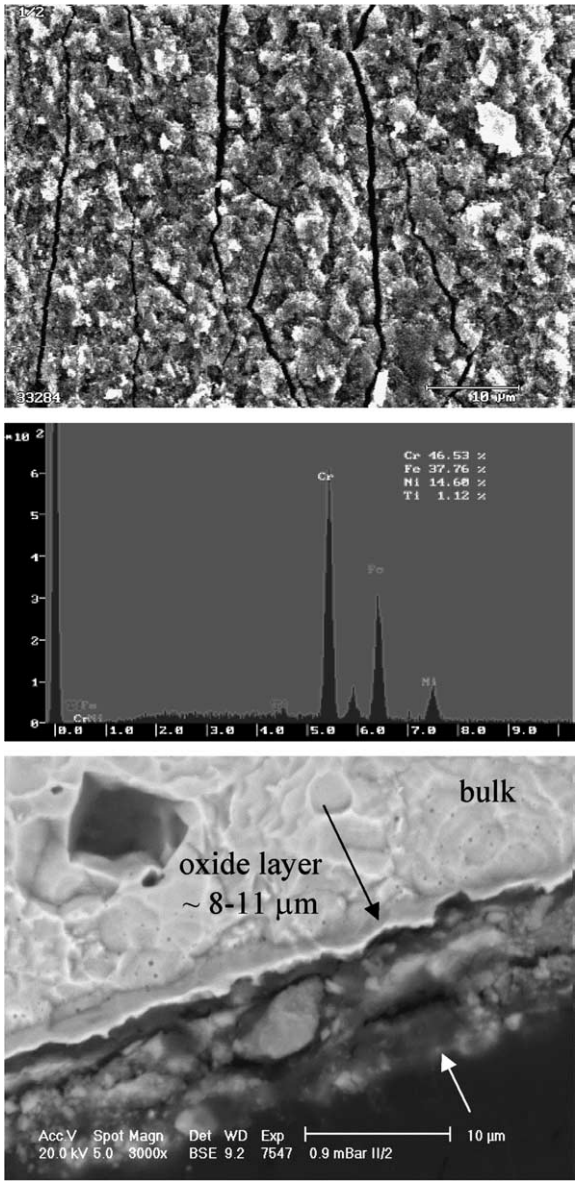

Fig. 5. An illustrative SEM micrograph ($M = 3000\times$), an EDX spectrum and an image of the metallographic cross-section (at the bottom) of the sample 4, representing samples decontaminated a few year before the sampling.

3–5 μm and crystalline remnants could be seen. As the inner surface of this sample was decontaminated right before the sampling, *it is concluded that the manganese – probably in the form of MnO_2 – remained on the surface following the AP-CITROX decontamination procedure*.

On the surfaces of samples never decontaminated (Nos. 10, 14–21), as well as of the inactive reference sample (22) there is a thin grown-on oxide layer

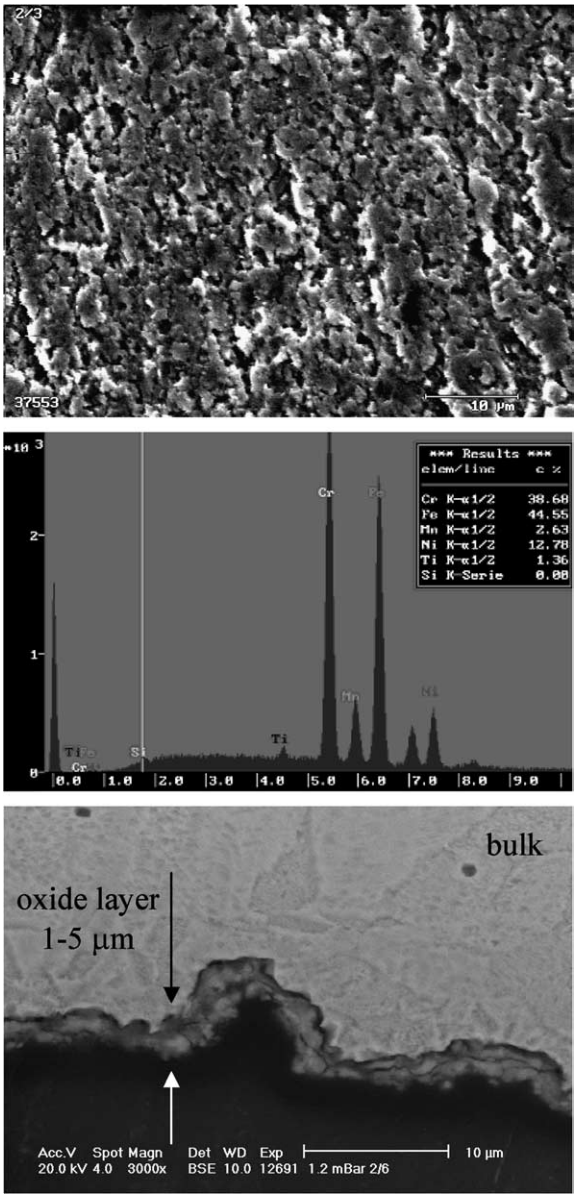

Fig. 6. An illustrative SEM micrograph ($M = 3000\times$), an EDX spectrum and an image of the metallographic cross-section (at the bottom) of the sample 7, representing samples decontaminated one or two years before the sampling.

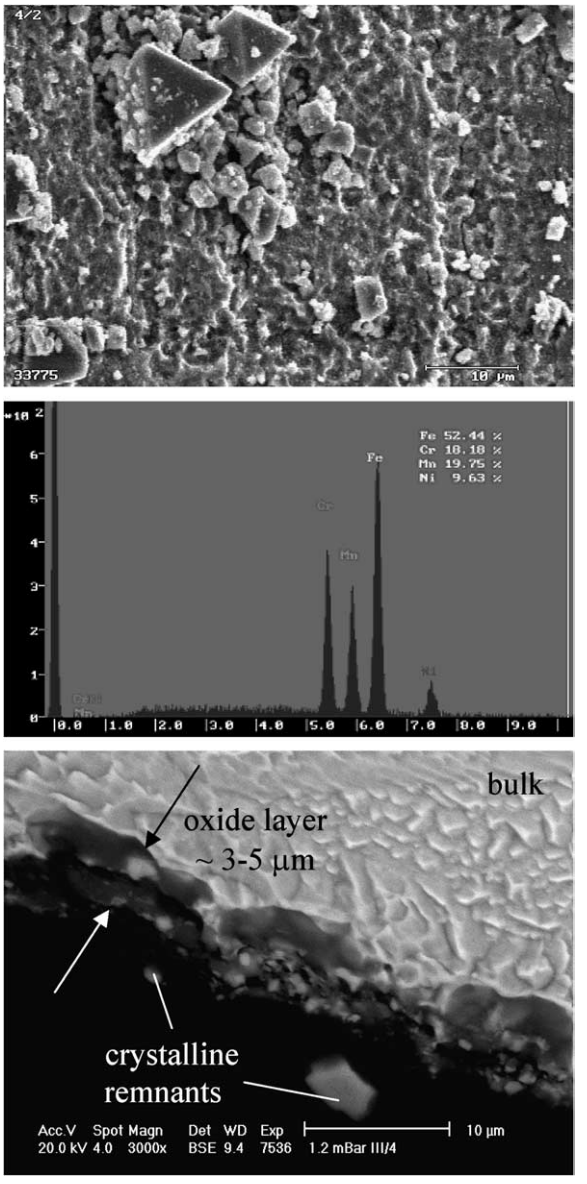

Fig. 7. An illustrative SEM micrograph ($M = 3000\times$), an EDX spectrum and an image of the metallographic cross-section (at the bottom) of the sample 12, representing samples decontaminated right before the sampling.

with excellent protective character. In the majority of these oxide films cracks cannot be identified and large amounts of less-adhered crystalline phases (presumably magnetite and hematite) are deposited on top of the grown-on layers. SEM–EDX data measured on the inner surface of sample 18 and the metallographic cross-section of that, characteristic for this group of the samples, are shown in Fig. 8.

The metallographic cross-sections of tube specimens were also studied to evaluate some quantified parameters for the oxide layers (such as thickness of the surface films, ratio of the cracks, main constituents of the oxide structure). Illustrative and multi region segmented SEM images of some selected samples 8, 9 and 16 are shown in Fig. 9. The quantified parameters of these images and modeling of the weight of oxide layer formed on

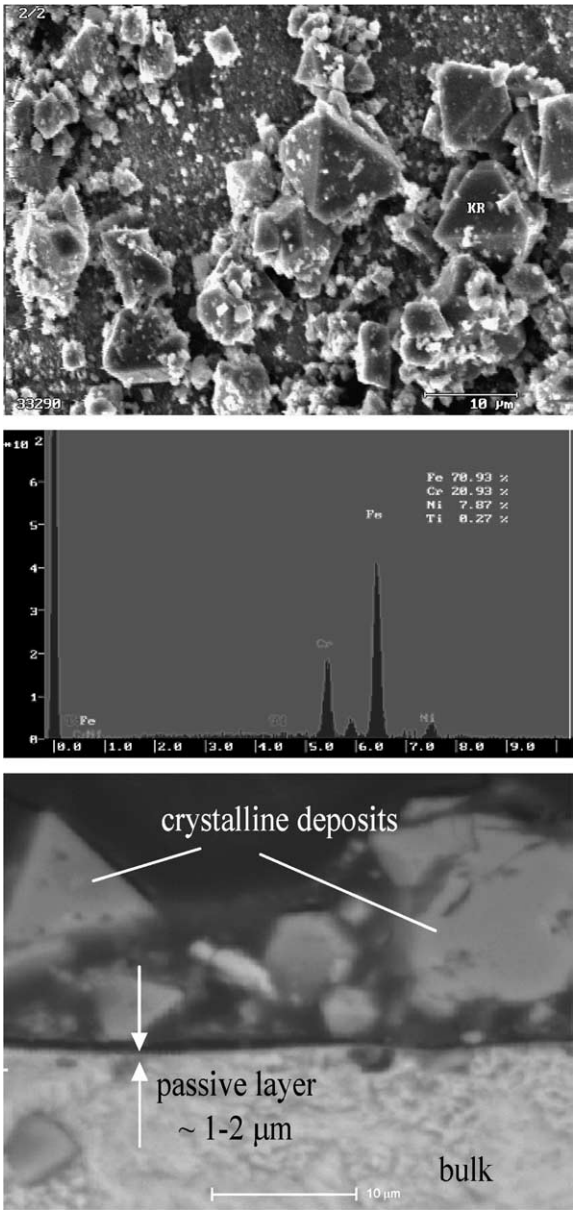

Fig. 8. An illustrative SEM micrograph ($M = 3000\times$), an EDX spectrum and an image of the metallographic cross-section (at the bottom) of the sample 18, representing samples never subjected to decontamination.

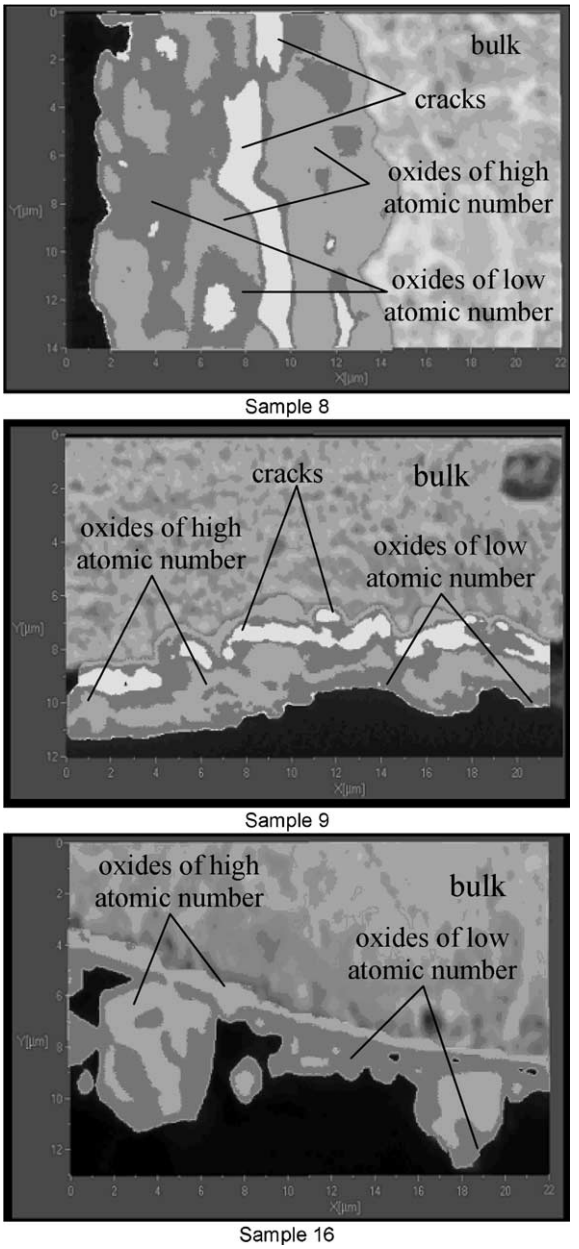

Fig. 9. Illustrative images of the SEM micrographs of the metallographic cross-sections utilized for image analysis.

inner surfaces of three SGs are given in Tables 3 and 4. The ratio of the cracks to the entire inner surface area provides information on the hypothetical stability and mobility of the oxide layer. The calculated constituents (components of low and high average atomic number) are necessary to evaluate the solution concentration and contact time in the pre-oxidizing process, while the estimated amount of Fe is essential to adjust the solution concentration and contact time in the reductive dissolution step to be developed for a regenerative version of the AP-CITROX decontamination technology. Data fit to iron mass distribution are ranging from 5.71 kg to 64.37 kg, the average value is ca. 22 kg.

Table 3
The quantified parameters for the oxide layer and the cracks obtained from the SEM micrographs of metallographic cross-section of samples 8, 9 and 16

Sample	Magnification	Oxides of low atomic number		Oxides of high atomic number		Cracks		Total oxide layer area (μm^2)
		Area (μm^2)	Ratio	Area (μm^2)	Ratio	Area (μm^2)	Ratio	
8	5000	68.7	39.08	86.0	48.92	21.1	12.00	175.8
9	5000	29.6	45.05	24.7	37.60	11.4	17.35	65.7
16	5000	49.2	63.57	28.2	36.43	–	–	77.4

Table 4
Estimation of the volume, weight and iron mass of oxide layers grown-on tube samples (SGs) 8, 9 and 16

Sample (SG)	Oxides of low atomic number			Oxides of high atomic number			Total Fe (kg)
	Volume (m^3)	$Fe(OH)_3$ (kg)	Fe (kg)	Volume (m^3)	Spinel-type oxide (kg)	Fe (kg)	
8	9.8967E − 03	35.63	18.63	1.2389E − 02	67.01	45.74	64.37
9	2.8913E − 03	10.41	5.44	2.4126E − 03	13.05	8.91	14.35
16	4.6253E − 03	16.65	8.71	2.6511E − 03	14.34	9.79	18.49

5. Discussion

Based on the general corrosion characteristics and applying multivariate cluster analysis (corrosion rate, thickness and chemical composition of the protective oxide layer) the samples studied may be classified into three groups. These are as follows:

- The corrosion rates measured in boric acid at the inner surface of the samples that were never subjected to decontamination (Nos. 10, 14–21) are extremely low ($v_c \leqslant 0.8$ μm year^{-1}), these values are actually below the reference ones measured by the Russian designers for this type of steel in water at 280–350 °C [4,19]. The average corrosion rate of these samples is about the same as that of the inactive reference sample (No. 22). The thin passive-layer of a thickness up to 1–2 μm grown-on the base alloy exhibits excellent protective behavior. This film is mostly free of cracks and covered predominantly by crystalline deposits (probably magnetite and hematite). The development of a less-adhered crystalline deposit layer is considerable on the overall surface of every sample.
- A satisfactorily protective oxide layer was found on the inner surface of the samples which were decontaminated by the AP-CITROX procedure a long time before the sampling (Nos. 3, 4 and 13.). However, the average corrosion rates measured at their inner surface in boric acid coolant were much larger ($v_c \geqslant 2$ μm year^{-1}) than those of the samples discussed above. The oxide layer grown-on their surface is thick (thickness 8–11 μm) and compact, nevertheless many cracks and scattered deep damages can be identified on the surface film. No presence of any crystalline deposits could be identified.
- In the case of samples Nos. 1, 2, 5–9 and 11 which were investigated about one or two years after decontamination (see Table 1), the structure and corrosion state of the oxide films are found to be a *mixture of the above two groups of specimens*. The average corrosion rates measured at their inner surfaces in boric acid are low ($v_c \leqslant 0.8$ μm year^{-1}), which are similar to those of samples never subjected to decontamination. On the other hand, a medium thick or thick (thickness $\geqslant 1$ μm) oxide layer with microheterogeneous character can be found on the inner surface of every sample. No presence of any crystalline deposits, nevertheless some cracks and damages (craters) can be observed on the surface.

6. Conclusions

Within the frame of a comprehensive program to qualify the general corrosion state of heat exchanger tubes, corrosion and metallographic features of 22 specimens originating from different SGs of the Paks NPP were studied by electrochemical

(voltammetry) and surface analyzing (SEM–EDX) methods. Despite the limited number of tube samples, some general conclusions can be drawn.

The heat exchanger tubes of the SGs may be classified into three groups. In the case of tube samples that were never subjected to decontamination the corrosion rates measured are very low and a coherent passive-layer of a thickness up to 2 μm is usually formed on their inner surfaces after various periods of normal operation. In contrast, corrosion rates measured at the decontaminated samples are notably higher and the oxide layer grown-on their inner surfaces is thick (up to 11 μm). Moreover, a strong dependence of the measured corrosion characteristics (corrosion rate, thickness and chemical composition of the protective oxide layer) on the decontamination history of the steam generators is revealed. It is well documented that the chemical decontamination carried out by a non-regenerative version of the AP-CITROX procedure does exert, on the long run, a detrimental effect on the corrosion resistance of steel surfaces.

Finally, it should be noted that adverse effects (general attack, formation of '*hybrid*' layer with accelerated corrosion rate and great mobility) of the chemical decontamination on the corrosion state of the inner surface of the heat exchanger tubes has been interpreted in [4,21]. The formation of *a* '*hybrid*' *structure of surface oxides* is supported by the results of the CEMS, XRD and XPS studies, which shall be discussed in the second part of the present work.

Acknowledgements

This work was supported by the Paks NPP Co. Ltd. (Paks, Hungary), and the Hungarian Science Foundation (OTKA Grant No.T 047219/2004).

References

[1] T. Katona, S. Rátkai, Á. Bíró Jánosiné, Cs. Gorondi, Fizikai Szemle 11 (2001) 341.
[2] D. Bodansky, Nuclear energy, AIP Press Woodbury, New York, 1996.
[3] J. Lipka, V. Slugen, I. Toth, J. Hascik, M. Lehota, Hyp. Interact. 139/140 (2002) 501.
[4] K. Varga, The role of interfacial phenomena in the contamination and decontamination of nuclear reactors, in: G. Horányi (Ed.), Radiotracer Studies of Interfaces, Interface Science and Technology, Vol. 3, Elsevier B.V., Amsterdam, 2004, p. 313.
[5] K. Varga, Z. Németh, A. Szabó, D. Oravetz, P. Tilky, J. Schunk, Magy Kém. Folyóirat 108 (2002) 444.
[6] Z. Homonnay, E. Kuzmann, S.K. Sticleutner, É. Makó, K. Varga, Z. Németh, A. Szabó, P. Tilky, J. Schunk, G. Patek, Magy Kém. Folyóirat 108 (2002) 449.
[7] K. Varga, P. Baradlai, G. Hirschberg, Z. Németh, D. Oravetz, J. Schunk, P. Tilky, Electrochim. Acta 46 (2001) 3783.
[8] K. Varga, Z. Németh, J. Somlai, I. Varga, R. Szánthó, J. Borszéki, P. Halmos, J. Schunk, P. Tilky, J. Radioanal. Nucl. Chem. 254 (3) (2002) 589.
[9] Z. Homonnay, A. Vértes, E. Kuzmann, K. Varga, P. Baradlai, G. Hirschberg, J. Schunk, P. Tilky, J. Radioanal. Nucl. Chem. 246 (1) (2000) 131.
[10] Z. Homonnay, E. Kuzmann, K. Varga, J. Dobránszky, A. Vértes, P. Baradlai, G. Hirschberg, J. Schunk, P. Tilky, Hyp. Interact. 139/140 (2002) 215.
[11] G. Hirschberg, P. Baradlai, K. Varga, G. Myburg, J. Schunk, P. Tilky, P. Stoddart, J. Nucl. Mater. 265 (1999) 273.
[12] M. Prazska, J. Retbarik, M. Solcanyi, R. Trtilek, Czech. J. Phys. 53 (2003) A687.
[13] C.J. Wood, Prog. Nucl. Energ. 23 (1990) 35.
[14] J.A. Ayres, Decontamination of Nuclear Reactors and Equipment, The Ronald, New York, 1970, pp. 483.
[15] M. Balaskó, F. Korösi, E. Sváb, I. Eördögh, Nucl. Instrum. Methods Phys. Res. A 424 (1999) 263.
[16] F. Korösi, M. Balaskó, E. Sváb, Nucl. Instrum. Methods Phys. Res. A 424 (1999) 129.
[17] M. Balaskó, M. Jancso, F. Korösi, Appl. Radiat. Isotopes 61 (4) (2004) 597.
[18] M. Balaskó, F. Korösi, Zs. Szalay, Appl. Radiat. Isotopes 61 (4) (2004) 511.
[19] V.V. Geraszimov, A.Sz. Monahov, A nukleáris technika anyagai (in Hungarian), Műszaki Könyvkiadó, Budapest, 1981.
[20] J. Hair, R. Anderson, R. Tatham, Multivariate Data Analysis, third ed., Prentice-Hall, Englewood Cliffs, NJ, 1992.
[21] A. Szabó, K. Varga, Z. Németh, K. Radó, D. Oravetz, Mrs. K. É. Makó, Z. Homonnay, E. Kuzmann, P. Tilky, J. Schunk, G. Patek, Corros. Sci., in press.